International Journal of Fracture **71**: 273–291, 1995.

Quantifications of crack constraint effects in an austenitic steel

HUANG YUAN,[1] GUOYU LIN and ALFRED CORNEC
[1] *Current address: Research Center Neumünster, NU TECH GmbH, 24536 Neumünster, Germany*
GKSS-Research Center, Institute for Materials Research, 21502 Geesthacht, Germany

Received 4 January 1994; accepted in revised form 8 November 1994.

Abstract. In this paper we studied the quantitative assessment of the constraint effects at the crack-tip fields in an austenitic stainless steel (X6CrNi1811). The $J-Q$ annulus was verified in two-dimensional crack fields under both small-scale and general yielding conditions. Four different geometries with shallow through deep cracks were studied. It has been shown that the Q values versus the J-integral are strongly dependent on the stress-strain curve. $J-T$ gives an accurate description of the crack-tip state only at low load. In three-dimensional crack analysis, the stress fields tend towards the plane stress solution in both thick and thin specimens. The specimen thickness thus plays a key role in characterisation of the three-dimensional crack-tip fields. The second terms in the three-dimensional stress fields depend on distance to the tip and to the free edge-surface of the specimen. It has been shown that the stress triaxiality at the crack tip is essentially a linear function of Q. In the CT specimens examined, Q locally characterises the stress triaxiality at the three-dimensional crack-tip front fields.

1. Introduction

The effect of stress constraint at the crack tip has been extensively studied for several years and has become one of the keen topics in recent fracture mechanics research. Through extensive finite element calculations, Hancock and co-workers [1, 2] have shown that the loading in-plane biaxiality significantly affects the stress fields at the crack tip. Parks and Wang [3, 4] have discussed three-dimensional crack-tip fields in shallow-cracked panels and suggested that the $J-T$ description might be simply generalised to assess the constraint effects in the three-dimensional crack fields in the ductile fracture process. In this case, it is interesting to clarify what T in the general yielding case means and how it should be calculated [3, 4].

A different approach to quantify the hydrostatic stress state at the crack tip has been suggested by O'Dowd and Shih [6, 7, 8]. They have examined the characteristics of the high and low stress triaxialities surrounding the finite strain zone and introduced the $J-Q$ annulus in the framework of the J_2-deformation/flow theory of plasticity. In their studies the elementary plane strain solution based on the modified boundary layer formulation, $[\sigma_{ij}]^{\mathrm{SSY},T=0}$, was taken as the reference solution. The second term was obtained by subtracting the reference solution scaled by the applied J from the full-field solution, i.e.

$$\sigma_{ij} = \left[\sigma_{ij}\left(\frac{r}{J/\sigma_0}, \theta\right)\right]^{\mathrm{SSY},T=0} + Q\sigma_0\hat{\sigma}_{ij}(r,\theta), \tag{1}$$

where J is Rice's J-integral [9] and σ_0 the yield stress. In the above equation the first term characterises the stress gradient, while the second one scaled by the factor Q determines the level of the stress curves in the far-fields. $\hat{\sigma}_{ij}$ is generally a function of both polar coordinates, r and θ, centred at the crack tip. Under the J_2-deformation theory of plasticity with Ramberg–

Osgood model, O'Dowd and Shih [6, 7] have found the second term in (1) may be replaced by the Kronecker-delta,

$$\sigma_{ij} = \left[\sigma_{ij}\left(\frac{r}{J/\sigma_0}, \theta\right)\right]^{\mathrm{SSY},T=0} + Q\sigma_0\delta_{ij}, \tag{2}$$

in the forward sector ($|\theta| < \pi/2$), where the dimensionless parameter

$$Q = \frac{\sigma_{\theta\theta} - \sigma_{\theta\theta}^{\mathrm{SSY},T=0}}{\sigma_0} \quad \text{at} \quad \frac{r}{J/\sigma_0} = 2, \theta = 0, \tag{3}$$

defines a measure of the near-tip stress triaxiality, or crack-tip constraint, relative to a reference high triaxiality stress state. This point has been convincingly confirmed by the higher-order asymptotic solution with four- or even five-term expansions by Xia et al. [12].

In the present paper we discuss quantification of constraint effects in an austenitic steel (X6CrNi1811). This is a very ductile material with high plastic capacity. Its J-integral value for crack initiation is about 400–500 N/mm at room temperature. In experiments performed at room temperature [13], it has been observed that the fracture processes are accompanied by a large amount of plastic deformation and obvious side-necking. This implies that the fracture occurs combined with strong out-of-plane constraint effects. To examine constraint effects in this strong ductile material, we have analysed crack-tip fields under both small-scale yielding and general yielding conditions. Four different geometries with varying crack lengths have been studied systematically. It has been shown that in general yielding cases, the Q values in the austenitic steel may be several times higher than those for the J_2 Ramberg–Osgood model. The absolute Q values increase significantly with the plastic zone growth. Furthermore, we have discussed constraint effects in the three-dimensional crack-tip front fields containing significant plane stress components. It has been found that the hydrostatic stress at $r/(J/\sigma_0) = 2$ and $\theta = 0$ can generally be approximated by a linear function of Q in the specimens investigated. Thus, Q may locally characterise the stress triaxiality at the crack tip.

2. Small-scale yielding results

To study constraint effects under small-scale yielding conditions, a modified boundary layer formulation may provide detailed information about the crack-tip fields at different loading biaxialities. In the boundary layer formulation, the remote traction is given by the first two terms of the linear elastic solution of Williams [11], which reads

$$\sigma_{ij} = \frac{K}{\sqrt{2\pi r}} f_{ij}(\theta) + T\delta_{1i}\delta_{1j}, \tag{4}$$

where K denotes the elastic stress intensity factor. f_{ij} is the non-dimensionalized angular function of the elastic stress fields. Using dimensional analysis one can easily show that the elastic-plastic crack tip stress fields must be of the form

$$\sigma_{ij} = \sigma_0 F_{ij}\left(\frac{r}{J/\sigma_0}, \theta, \tau; \text{ material properties}\right) \tag{5}$$

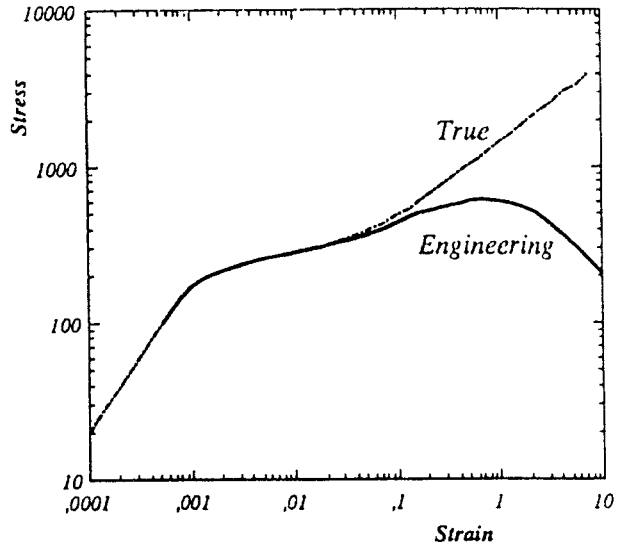

Fig. 1. Stress-strain curve used for finite element calculations. The solid curve denotes the engineering stress-strain relation, whereas the dash dot line represents the *true* stress-strain curve.

where F_{ij} is a dimensionless tensor valued function and the stress amplitude factor is represented by the J-integral. Under small-scale yielding conditions, the dimensionless functions depend only on the loading biaxiality ($\tau = T/\sigma_0$).

In the present work the investigated material, the austenitic steel is strongly nonlinear and has very different plastic strain-hardening at different stress levels (Fig. 1). In the figure the solid curve represents the engineering stress-strain relation in double-logarithmic coordinates, whereas the dash dot line means the *true* stress-strain curve. Both curves have been measured experimentally. The nonlinear deformation begins at a stress $\sigma_0 = 100\,\mathrm{N/mm^2}$ ($\varepsilon_0 = \sigma_0/E = 1/195$) and develops with the strain increasing continuously. The 0.2 percent plastic strain is measured at a stress $\sigma_{0.2} = 237\,\mathrm{N/mm^2}$ and afterwards the plastic strain increases rapidly. At 3 percent plastic strain the strain-hardening grows significantly and the true stress-strain curve may be approximated by a potential function with an exponent $n \to 2$. The Young's modulus is 195000 MPa.

The ABAQUS general-purpose finite element program [14] has been used for the computations. In all finite element calculations the J-integral has been calculated by the virtual crack extension method, which is implemented in ABAQUS. In finite deformation analysis the crack tip is assigned a finite root radius. In the two-parameter boundary layer analysis, the initial notch radius is assumed to be 10^{-5} times the distance to the remote boundary at which the traction is applied. According to the results of McMeeking and Parks [15], once the crack tip has been blunted to about 3 times the initial notch root radius, the solutions are not affected by the initial root radius. The radial length of the smallest elements is about $10^{-6}a$, where a denotes the crack length which is represented by the remote radius R in the boundary layer formulation (Fig. 2(a)). The mesh in the radial direction is generated by exponential scaling. Because of symmetry we only have to model the upper plane. The finite element model is constructed using 8-nodal isoparametric elements with reduced 2×2 Gaussian integration. There are 24 elements within the angular region from 0 to π in the crack-tip region.

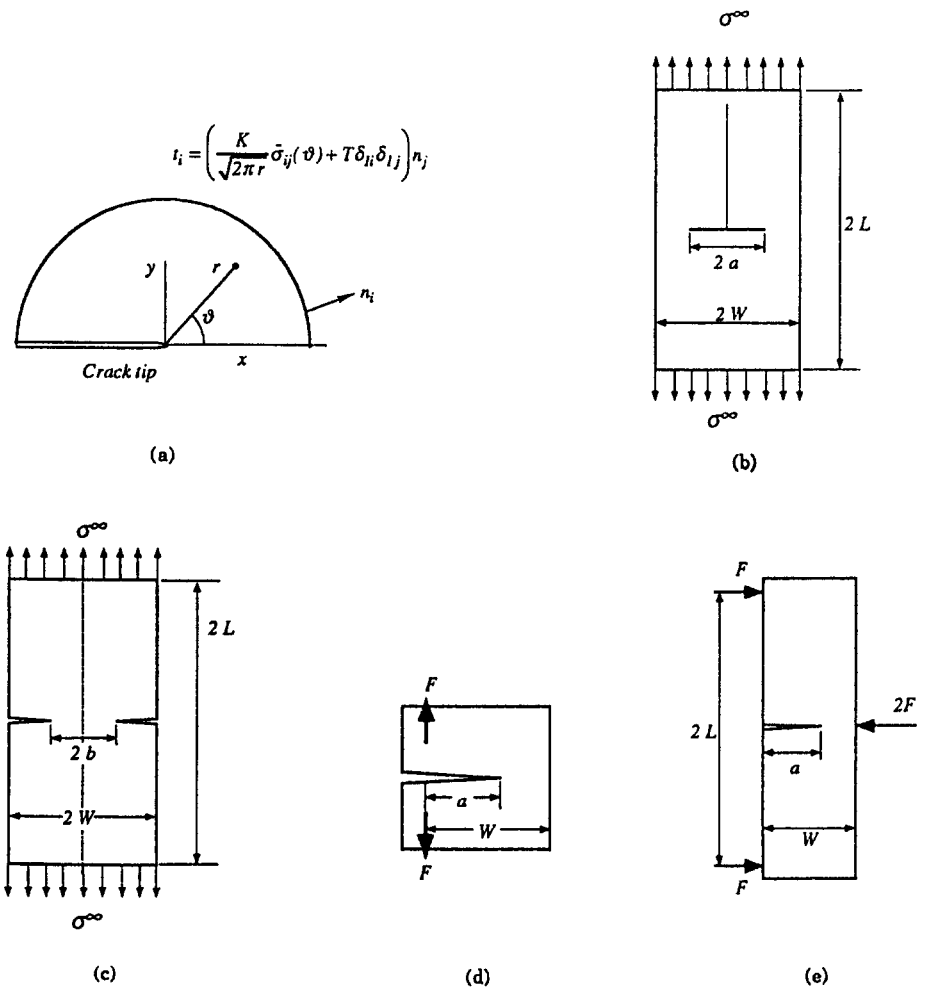

Fig. 2. Fracture specimen geometries: (a) modified boundary layer formulation (MBLF), (b) center-cracked panel (CCT), (c) double-edge cracked panel (DECP), (d) compact tension specimen (CT), (e) three-point bend bar (SENB).

In the modified boundary layer formulation, the displacement field of Williams [11] has been applied at the remote circular boundary of distance R, as shown in Fig. 2(a). The load level is controlled by the mode I stress intensity factor K in (4). In analogy to analyses under the J_2-deformation theory [6], the small-scale yielding stress distribution depends only on the value of the normalised transverse T-stress. Evaluation of the J-integral is not substantially affected by the applied T values when the crack fields are under monotonic loading conditions. The small-scale yielding conditions are enforced by not allowing the plastic zone r_p to exceed 0.1 R. The analysis of the boundary layer formulation with T-stress in the range $-1 < \tau < 1$ is considered.

Figure 3 displays the radial distribution of the in-plane normal stresses obtained in the finite element computations along the radial lines $\theta = 3.2°$. The stresses are taken from the Gaussian integration points near the ligament and the radial distance from the tip is calculated in the Lagrangian coordinates. The solid lines denote the reference solution with $T = 0$. Note that J/σ_0 is the relevant length scale on the order of CTOD. The stress and strain distributions

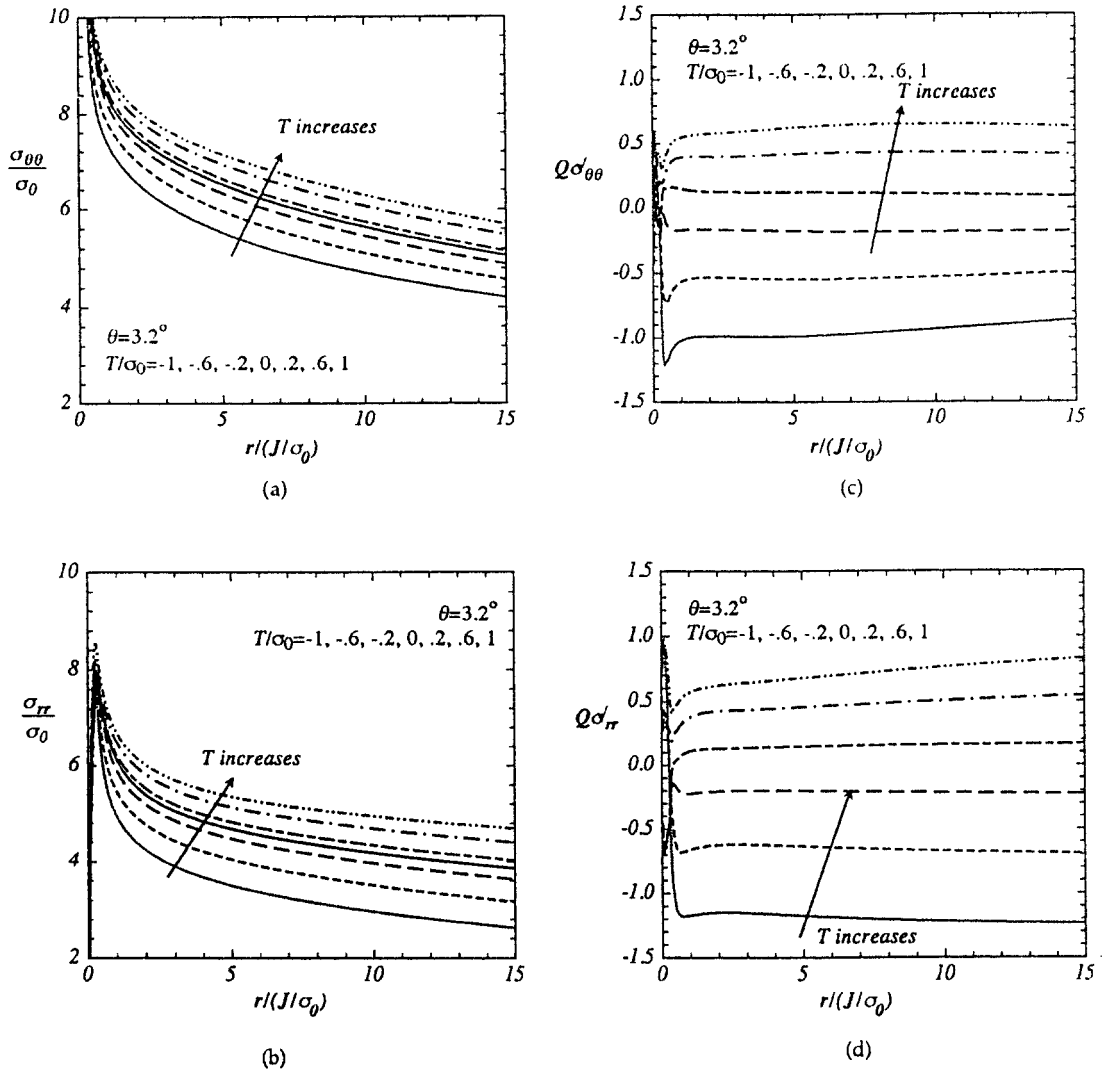

Fig. 3. Radial distributions of the in-plane stresses and the second terms under small-scale yielding conditions.

with the same T-stress value collapse onto a single curve, independently of the applied K values, when the distance from the tip is normalised by J/σ_0. The stresses at the crack tip are affected by the transverse T-stress as observed in all other materials. Due to high strain hardening in the large strain region, the finite strain affected zone is significantly smaller than that in the Ramberg–Osgood materials [15, 16]. Peaks of the normal stresses are so high that they reach thirty times the yield stress, σ_0.

The results from the austenitic steel (Fig. 4) show that the positive T-stress affects the triaxiality at the tip more significantly than that for the Ramberg–Osgood materials as reported by Shih and co-workers [6, 17, 18]. Figure 3(c,d) display the second term of the in-plane stresses in (1) which is essentially independent of the distance to the tip in the austenitic steel. Angular variations of the in-plane normal stresses as well as their second terms at $r/(J/\sigma_0) = 2$ are plotted in Fig. 4. It is shown that the second terms of the normal stresses are distributed in analogy to the results in [6].

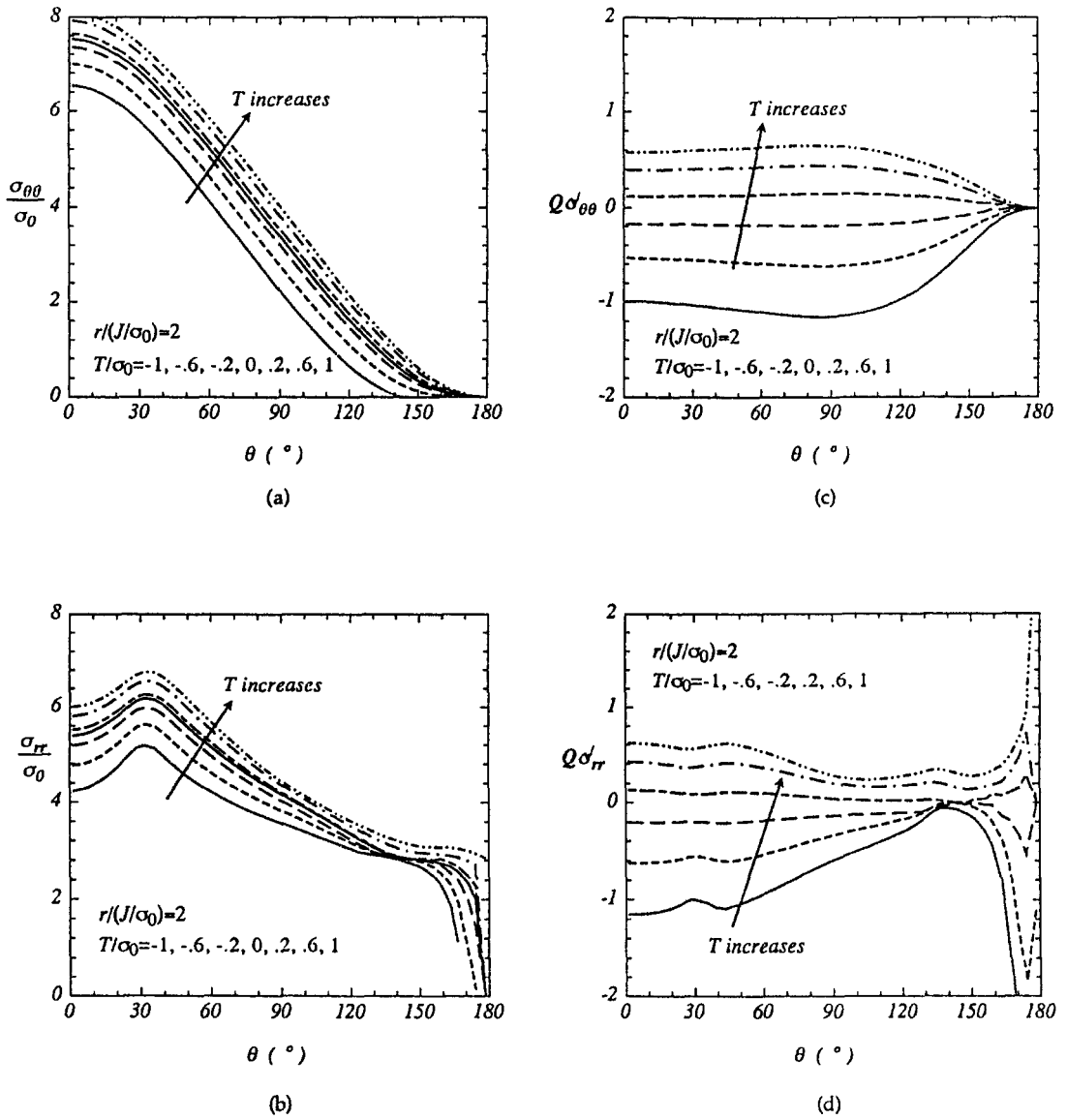

Fig. 4. Angular variations of the in-plane stresses and the second terms under small-scale yielding conditions.

From the curves in Fig. 4, it is seen that the maximum Q values defined in (3) may reach $+0.5$ for $\tau = 1$ and -1.0 for $\tau = -1$ under small-scale yielding conditions. There is a one-to-one correlation between the Q value and the applied loading biaxiality T. Q can be approximated through

$$Q = A\tau + B\tau^2 + C\tau^3, \tag{6}$$

where A, B and C have been listed in Table 1. The relation between T and Q under small-scale yielding conditions in the austenitic steel is shown in Fig. 5. The results of the Ramberg–Osgood materials with $n = 3$ and 10 in the figure are extracted from [17]. The figure reveals that Q locates between the two Ramberg–Osgood materials in the negative T region. For the

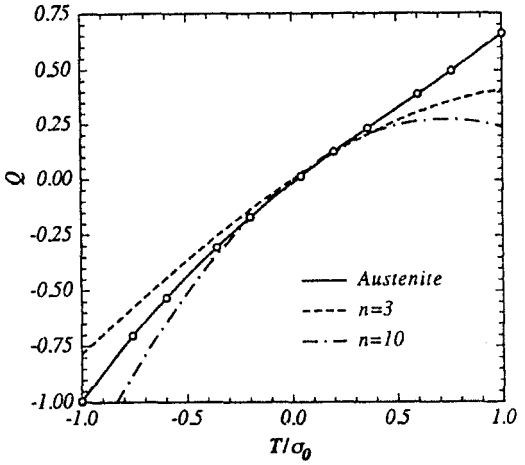

Fig. 5. Relationships between Q and T under small-scale yielding conditions. The results of the Ramberg–Osgood materials were reported in [6].

Table 1. The coefficients for the $T-Q$ relationship (6)

	Austenite	$n = 3$	$n = 10$
a_1	0.7374	0.6438	0.7594
a_2	−0.1523	−0.1864	−0.5221
a_3	0.09212	−0.0448	0

The results of the Ramberg–Osgood materials were reported in [17]

positive T-stress, however, the Q value grows significantly, whereas in the Ramberg–Osgood materials the growth gradient of Q decreases continuously.

3. Two-dimensional results under general yielding

The stress triaxiality at the crack tip can be quantified by an elastic field parameter (e.g. K and T) only when the material nonlinearity in the crack-tip field can be correlated by the elastic solution. As soon as the material plasticity characterises the whole crack field, the stresses at the crack tip cannot directly be controlled by the T terms, whereas the Q factor is a direct measure of the stress difference at the tip. Wang [4] has shown in his finite element computations of the surface-cracked panels under J_2 deformation theory that the tangential crack-tip front stress can be correlated by T indirectly. In [4] the reference stress fields are the boundary layer results with a suitable transverse T stress under plane strain conditions. Wang found that the three-dimensional crack-tip front fields could be approached by the plane strain boundary layer formulation. This T value should correlate the three-dimensional crack-tip fields under general yielding conditions according to his predictions. Whereas the Q evaluation requires detailed finite element calculations, the T-values could be simply determined from the applied stress intensity factor [20, 22] or the corresponding J-integral value, should the predictions

in [4] be generally valid for the fully plastic crack-tip fields. From this point of view, Parks [3] stated that $J-T$ appeared more convenient in quantifying the crack constraints than the $J-Q$ annulus. From the physical significance of Q, however, the $J-T$ correlation requires a one-to-one dependence between Q and T for both small-scale and general yielding. According to the calculations of Wang [4] the crack-tip front fields in the surface cracked panels could be normalised by the stresses of the boundary layer formulation, that is, the relation of (6) should be valid under general yielding conditions. From crack analysis of elasticity it is known that the T-stress is linearly proportional to the applied loads. This dependence can be expressed in the form

$$T = \sigma^{\infty}\Sigma \text{ (geometry)}, \tag{7}$$

where Σ is a dimensionless geometric factor derived from elasticity theory and σ^{∞} a representative load magnitude. Leevers and Radon [20] as well as Sham [22] have obtained T solutions for a number of cracked geometries. Substituting (7) into (6) follows

$$Q = F\left(\frac{\sigma^{\infty}}{\sigma_0}; \Sigma, \text{ material properties}\right). \tag{8}$$

The dimensionless function F depends on the load magnitude, the elastic geometry factor and the material properties. Thus, Q based on the $J-T$ description could be evaluated as soon as the applied load magnitude is known. In this relationship, the Q values are only connected with the material plasticity through the boundary layer formulation. Equation (8) is a direct consequence of the $J-T$ characterisation. One may study the $J-T$ characterisation by examining the agreement or disagreement between the Q-values from the full-field finite element calculations and Qs from (8).

Four of the conventional fracture test specimens examined in the present work are shown in Figs. (2b,2e). The tension specimens, the centre-cracked panel (CCT) in Fig. 2(b) as well as the double-edge cracked panel (DECP) in Fig. 2(c), are loaded under uniaxial tension; the bend specimens, the three-point bend bar (SENB) in Fig. 2(e) and the compact tension panel (CT) in Fig. 2(d), are loaded by concentrated forces. We have examined shallow- through deep-cracked geometries for all specimens with $a/W = 0.1$, 0.3, 0.5, 0.7 and 0.9, respectively. A crack is designated a shallow crack when the relevant dimension is the crack length ($a/W \leqslant 0.5$) and a deep crack when the relevant dimension is the uncracked ligament ($a/W \geqslant 0.5$). All computations have been conducted under the infinitesimal deformation theory of incremental plasticity. The choice of material model will not affect our final predictions [5].

3.1. TENSION GEOMETRIES

Figure 6 shows angular variations of the hydrostatic stress at different load levels in the centre-cracked panel under plane strain conditions. The ratios of the crack length *(a/W)* are 0.1, 0.5 and 0.9, respectively. The fields are plotted at $r/(J/\sigma_0) = 2$. In the centre-cracked panel the hydrostatic stress at the crack tip shows considerable dependence on the applied J values. The angular variations are analogous in all applied load levels and for all crack lengths. With increasing load, the stress triaxiality in the whole crack-tip fields decreases uniformly. The hydrostatic stress near to the crack surfaces ($\theta = \pi$) falls increasingly into the hydrostatic compression state in the centre-cracked specimens. Due to the low yield stress of the austenitic steel as well as its high plastic strain-hardening, the maximum decrement of the

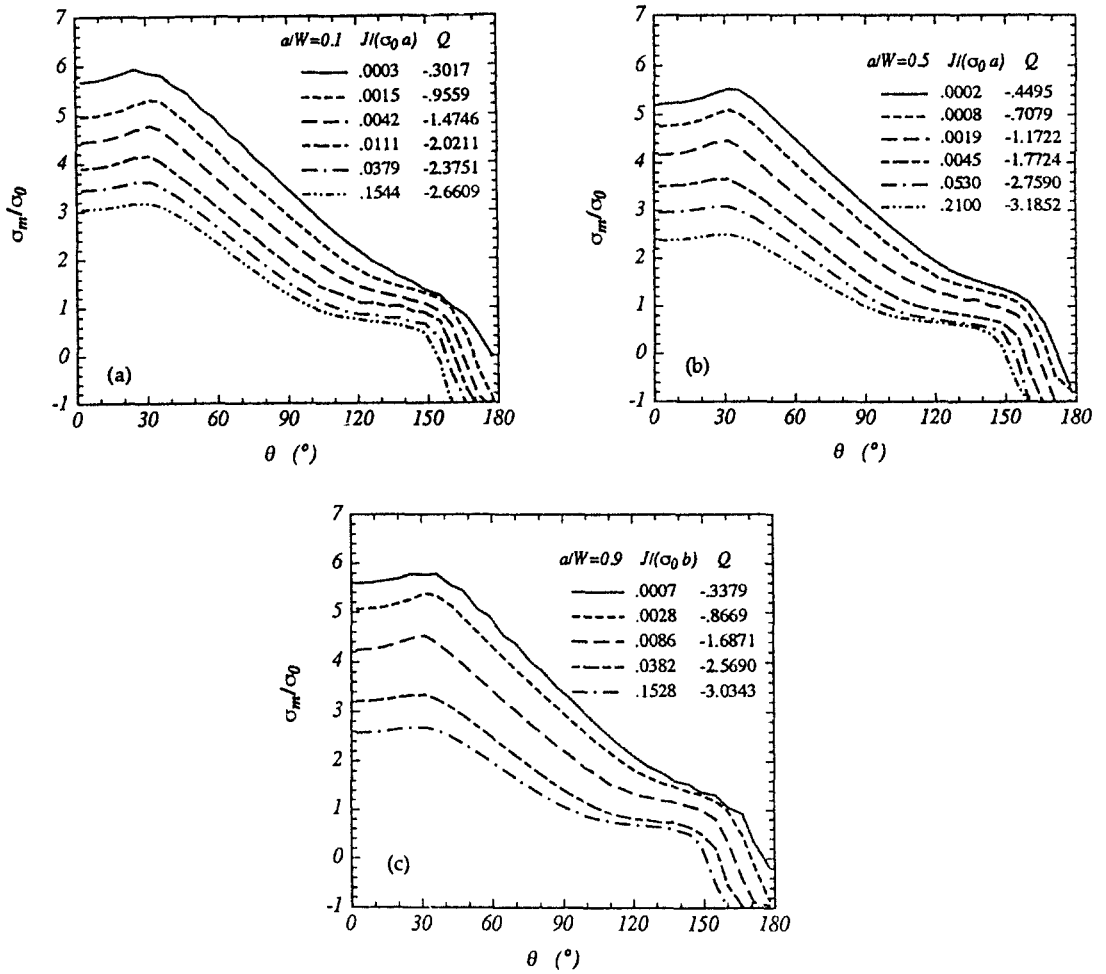

Fig. 6. Angular variations of the stress triaxiality around the crack tip at $r/(J/\sigma_0) = 2$ for the center-cracked panels (CCT) with $a/W = 0.1, 0.5$ and 0.9.

triaxiality may reach a value several times σ_0. These features have also been observed in the double-edge cracked panels.

The dependence of Q on the extent of plastic yielding measured by $J/(a\sigma_0)$ for the centre-cracked panels as well as the double-edge cracked panels $a/W \leqslant 0.5$ is plotted in Fig. 7. For $a/W > 0.5$ the corresponding plastic yielding is measured by $J/(b\sigma_0)$, as in [17]. Here b denotes the length of the uncracked ligament ($b = W - a$). Independently of crack length, all curves start at the small-scale yielding solutions and the constraints decrease with the applied loads. The constraints fall significantly when the plastic zone has grown through the uncracked ligament. Compared with the hydrostatic stress distributions in Fig. 6, Q gives a correct representation of the hydrostatic stress state at the crack tip. In CCT and DECP with $a/W < 0.7$, the Q curves are essentially independent of the crack length. They are, however, nonlinearly dependent on the applied loads.

In the figures the symbols denote Q evaluated from T. The corresponding T values are based on the results of [20]. By introducing the stress biaxiality ratio B [20], the normalised transverse stress can be expressed by

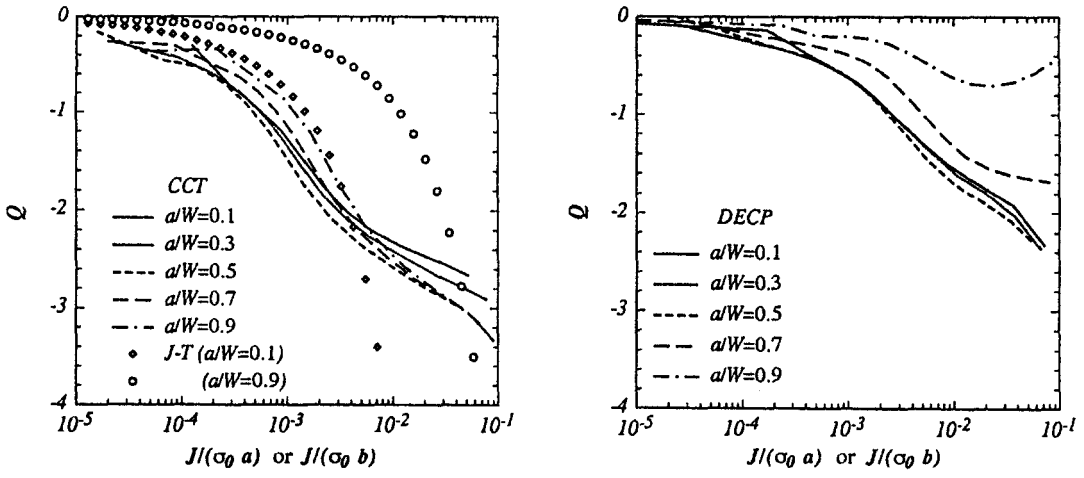

(a) (b)

Fig. 7. $Q-J$ relations for the tension geometry with different crack lengths ($a/W = 0.1, 0.3, 0.5, 0.7$ and 0.9). Q is defined in (3). The symbols denote the results calculated from the T-stress as suggested in [4]. (a) The center-cracked panels (CCT); (b) The double-edge cracked panels (DECP).

$$\tau = B\sqrt{\frac{E}{\pi\sigma_0(1-\nu^2)}\frac{J}{a\sigma_0}}. \tag{9}$$

For the center-cracked specimen Leevers and Radon [20] predicted that the stress biaxiality can be expressed as

$$B = -\left(1 + 0.085\frac{a}{W}\right). \tag{10}$$

This result implies that the stress biaxiality ratio at the crack tip in elastic CCT specimens is hardly affected by the crack length. τ is almost a single variable function of the load factor $J/(a\sigma_0)$ and so will be the corresponding Q's, which are calculated by making use of the boundary layer results under small-scale yielding conditions (6), as suggested by Wang [4].

This point is confirmed in Fig. 7(a) for $a/W \leqslant 0.5$, in which only the result with $a/W = 0.1$ is plotted, since there is graphically no difference between it and the curve with $a/W = 0.5$. A significant difference is observed at curve $a/W = 0.9$, which shows Q as a function of $J/b\sigma_0$, instead of $J/a\sigma_0$. This discrepancy is only caused through the variable transformation in the diagram ($J/a\sigma_0$ by $J/b\sigma_0$).

Compared with the finite element calculations, the $J-T$ prediction gives much too small a stress triaxiality at the tip in deep cracked panels. The curves have the same trend, but full-field results vary considerably less than T predicts. The T prediction approaches the correct Q values only at low load levels. Deviation between the full fields and the T solution grows as loads increase.

Due to high plastic hardening in the austenitic steel, the Q value grows rapidly after the plastic zone has spread out. This feature cannot be described by the $J-T$ description combined with the small-scale yielding solution. At the high load level, the T prediction deviates significantly due to restriction of the $Q-T$ relation (6). Variations of the stress triaxiality for different tension specimens and different load levels cannot be expressed by the small-scale yielding solutions.

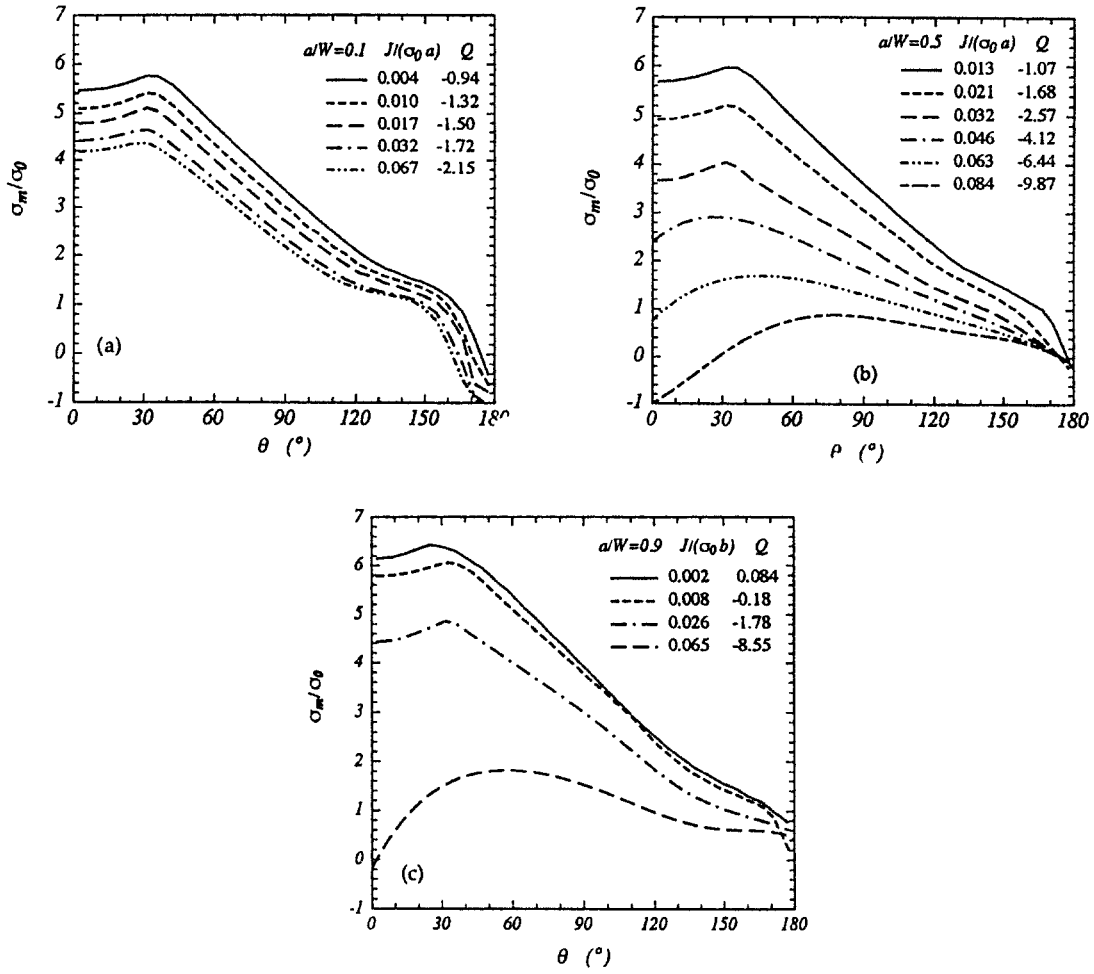

Fig. 8. Angular variations of the stress triaxiality around the crack tip at $r/(J/\sigma_0) = 2$ for the three-point bend bars (SENB) with $a/W = 0.1, 0.5$ and 0.9.

3.2. BEND GEOMETRIES

The bend specimens contain generally a higher stress triaxiality under fully plastic conditions. This difference from the tension specimens becomes significant even at very low load level. Figure 8 plots angular variations of the hydrostatic stress in three-point bend bars (SENB) with $a/W = 0.1, 0.5$ and 0.9 under different load levels, respectively. The fields are plotted at $r/(J/\sigma_0) = 2$. Before the plastic zone spreads over the uncracked ligament, the hydrostatic stress in the bending bars is slightly affected by the applied loads. As soon as the loads reach the plastic load level, the hydrostatic stress drops from that of the small-scale yielding solution rapidly. In comparison with the tension specimens, the deviations of the stress triaxiality due to the different loads are restricted mainly in the forward sector ($|\theta| < \pi/2$). The hydrostatic stress in the backward sector ($|\theta| > \pi/2$) is only slightly affected by the applied J values. This is a characteristic difference from the tension geometries. It implies that the hydrostatic stress in a fully plastic specimen is substantially affected by the load configuration and can only be characterised by an additional parameter ahead of the crack tip ($\theta = 0$). The definition

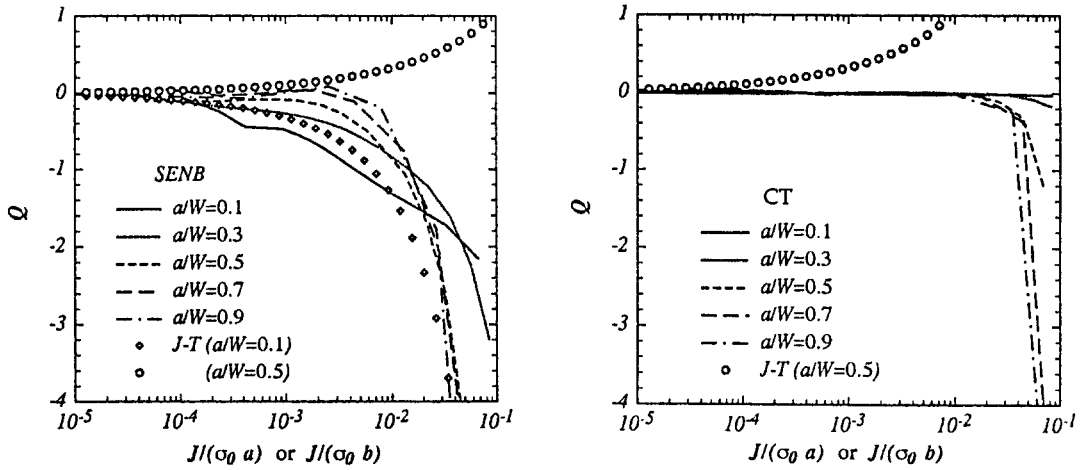

(a) (b)

Fig. 9. $Q-J$ relations for the bend geometry with different crack lengths ($a/W = 0.1, 0.3, 0.5, 0.7$ and 0.9). Q is defined in (3). The symbols denote the results calculated from the T-stress as suggested in [4]. (a) The three-point bending bars (SENB); (b) The compact tension specimens (CT).

of a characteristic parameter in finite geometry and where it is evaluated is not arbitrary. A parameter defined behind the crack tip ($\theta = \pi$) can not describe the stress variation at $\theta = 0$. From this point of view, the definition of Q in (3) is more relevant to the fracture process than a parameter evaluated behind the tip.

It is known that the crack-tip state in the bend bars is practically not affected by the applied load under small-scale yielding conditions. This feature can be clearly observed in development of the Q curves in Fig. 9, in which Q is plotted as a function of the load levels measured by $J/(a\sigma_0)$ for $a/W \leqslant 0.5$ or $J/(b\sigma_0)$ for $a/W > 0.5$. Whereas the Q values of the CT specimens up to $J/(\sigma_0 a)$ or $J/(\sigma_0 b)$ less than 0.012 almost exactly equal zero, the three-point bending bars show a slightly different stress triaxiality. Apart from the shallow cracked specimens, the bending geometries show weak dependence on the crack length at all load levels. In the shallow cracked CT specimens, Q development in the plastic load region appears to be strongly affected by the crack length. The two bend geometries show very different Q distributions with the applied loads.

In both bend specimens the elastic stress biaxiality ratio, B, [20] is an increasing function of the crack length. In SENB specimens, $B = 0.18$ for $a/W = 0.5$ and -0.48 for $a/W = 0.1$ (The latter value is extrapolated from the last four points of the results in [20]). The Q-curves predicted by T–J are plotted through the symbols in Fig. 9(a), as suggested by Wang [20]. The T prediction shows good agreement when the crack-tip fields are characterised by the small-scale yielding. As the plastic zone spreads over the whole uncracked ligament, T predictes two different developments of Q values for different crack lengths, while the finite element calculations show homogeneous variations. Similar features can be observed in the CT specimens (Fig. 9(b)), in which only elasticity prediction with $a/W = 0.5$ is plotted. One may conclude that there is not a one-to-one correlation between Q and T in the general yielding cases.

3.3. DISCUSSION

The numerical results above show that T gives a good estimate of the hydrostatic stress before the fully-plastic load level is reached. In the fully plastic state, T incorrectly predicts the triaxiality of the stress state ahead of the tip. The deviation from the full field results is proportional to the load amplitude. Q is not uniquely described by T under general yielding conditions, that is, the stress triaxiality at the crack tip is not correlated by the transverse T-stress. Similar observations have been reported in the Ramberg–Osgood materials [17]. In general yielding Q is increasingly affected by the geometry of the specimens and the load configuration, whereas T is essentially based on the linear elastic solution and/or the small-scale yielding observations, which exclude the local non-proportional plastic effects at the crack tip.

For finite width crack geometries, the results obtained from the modified boundary layer formulation can only be used under small-scale yielding conditions. The $J-Q$ annulus represents the variation of the crack-tip fields through the difference of the hoop stress ahead of the crack directly. With increasing applied J values, the crack-tip fields are affected by the finite specimen geometry. So (8) should be re-written in the form [17]

$$Q = F_{FP}\left(\frac{J}{\sigma_0 a};\ \text{geometry, material properties}\right) \tag{11}$$

under fully plastic conditions. The dimensionless function F_{FP} depends on the applied load $J/\sigma_0 a$, the specimen geometry and the material properties. Under plane strain conditions, Q generally represents the difference of the stress triaxiality at the crack tip.

4. Effects of three-dimensional fields on the $J-Q$ annulus

Numerical studies in [6, 17, 18] as well as in the present work have shown that Q characterises the crack-tip fields under plane strain conditions. It is confirmed in these works that the stress fields containing four stress components can be controlled by two parameters, J and Q. Under plane strain conditions the out-of-plane stress component σ_{zz} can be expressed through the two in-plane stresses. Additionally, the shear stress in the mode I fields is of secondary significance, so that there are practically only two independent stresses, σ_{xx} and σ_{yy}, to be characterised in the plane strain fracture process. It implies that the three-dimensional crack fields can be characterised by $J-Q$ accurately, only if the out-of-plane constraint effects may be represented by the in-plane parameter. A more detailed discussion about the constraint characterisation in three-dimensional crack-tip fields has been presented in [10] recently.

In [17] the Q values are slightly dependent on the distance to the tip in a surface-cracked tensile panel. From the calculations of Wang [4, 21] in similar cracked geometries this prediction is obvious, since the crack tip front fields are dominated by the plane strain solution. In general three-dimensional cases, however, all normal stresses are independent of each other. The out-of-plane stress component along the crack-tip front is strongly affected by the load level as well as the specimen thickness. Especially in thin plates, the crack-tip front fields may approach the plane strain fields only when the applied loads are limited in a very low level [19, 21]. Generally speaking, the three-dimensional crack fields are gradually dominated by the components of the plane stress fields as the applied load increases. It is of interest to know how the crack tip constraints are affected by variations of the out-of-plane stress component, if the crack-tip front fields are not dominated by the plane strain solution.

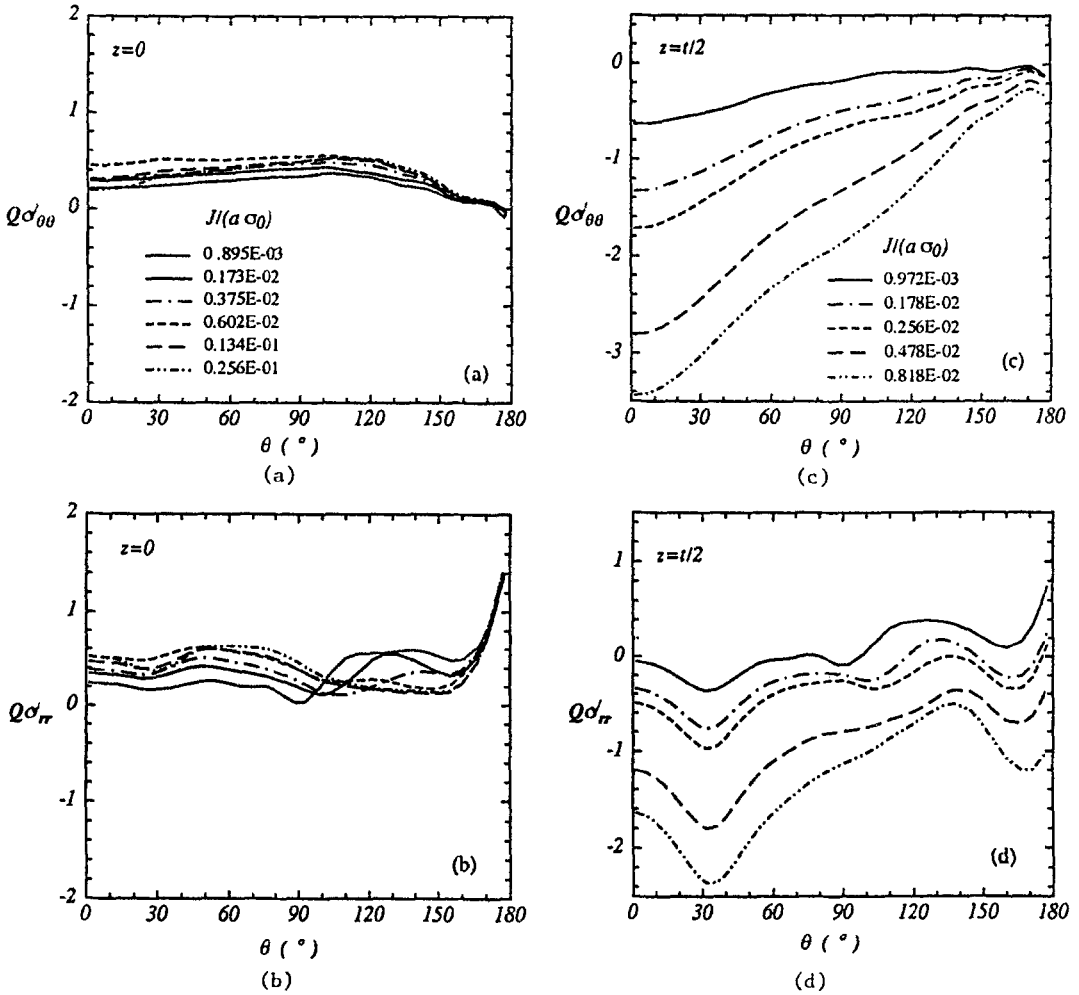

Fig. 10. Angular variations of the second-term of the normal in-plane stresses at the middle plane ($z = 0$) as well as near to the free surface ($z = t/2$) of the thick compact tension specimen (CT25) at $r/(J/\sigma_0) = 2$.

Numerical results of the two compact tension specimens ($W = 50$ mm, $a/W = 0.5$) of the austenitic steel are summarised in the present paper. The thicknesses of the specimens are 5 mm and 25 mm, respectively, which correspond to $1/5$ and $1/1$ of the uncracked ligament. The finite element model of the assumed geometry is loaded symmetrically. Only a quarter of the specimen has to be discretised. Both specimens are modelled by an analogous finite element mesh consisting of 6700 linear 8-nodal isoparametric elements with about 24000 degrees of freedom. Twelve fans of elements converge towards the crack tip. The finite element calculations have been performed under finite strain plasticity theory. The crack-tip blunting radius is assumed as 0.001 mm. The radial dimension of the smallest elements at the crack tip is approximately 10^{-5} mm. The discretization is sufficiently fine to permit adequate resolution of the stresses and strains within the crack-tip front fields (e.g. within ten crack-tip opening displacements). The three-dimensional J-integral values have been calculated using the virtual crack extension technique implemented in the general-purpose code ABAQUS [14]. Fifteen contours have been evaluated to obtain path-independence for the J-integral.

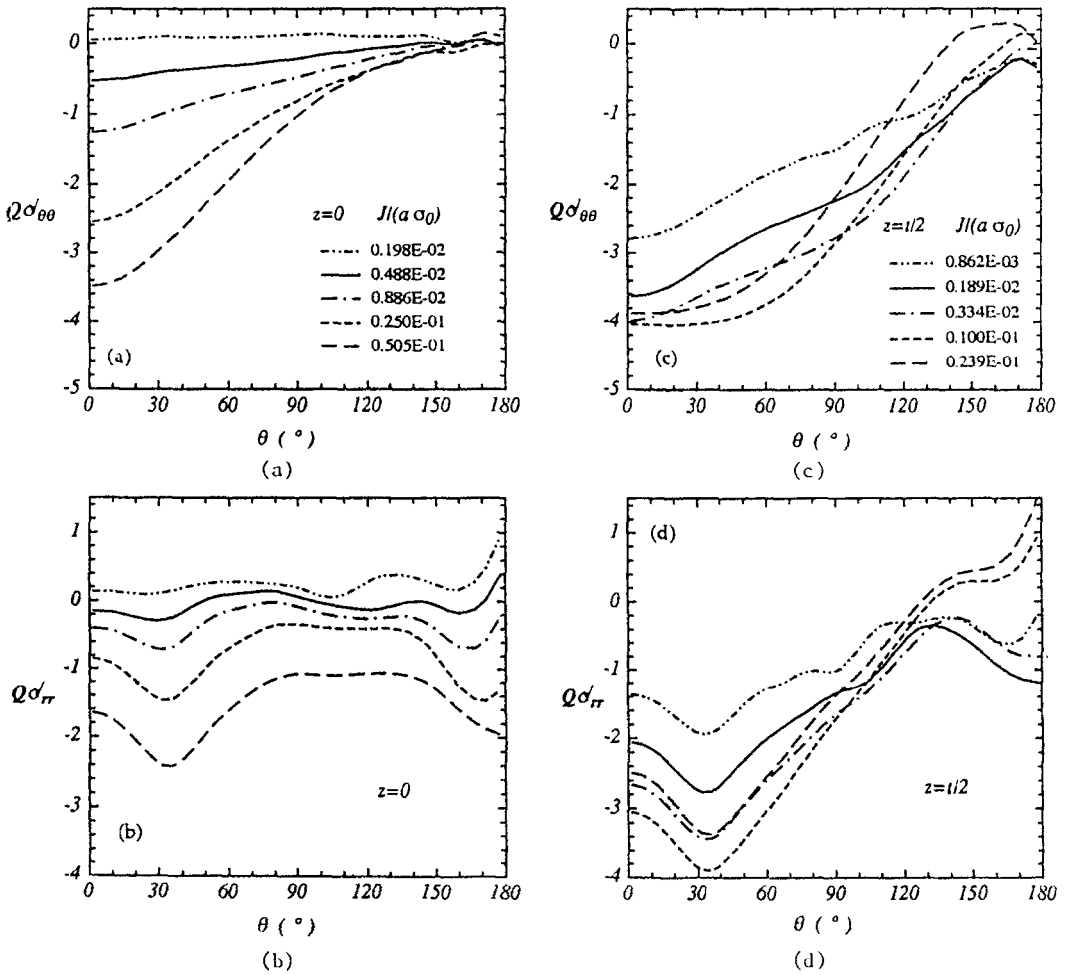

Fig. 11. Angular variations of the second-term of the normal in-plane stresses at the middle plane ($z = 0$) as well as near to the free surface ($z = t/2$) of the thin compact tension specimen (CT05) at $r/(J/\sigma_0) = 2$.

Nakamura and Parks [21] have shown that the crack-tip fields develop towards the plane stress fields as the plastic zone grows. Consequently, the difference between the full-stress fields and the reference solution (e.g. the plane strain small-scale yielding solution) depends significantly on the applied loads in the three-dimensional cracked geometry. Figure 10 plots distributions of the second terms defined in (1) with the polar angle in the thick specimen. In the figure the second terms of the in-plane stresses for the thick specimen are plotted at the middle plane ($z = 0$) as well as the free edge-surface ($z = t/2$), respectively. It is shown that the second-terms at the middle plane (Figs. 10(a,b)) are hardly affected by the applied J-integral even at high load level. The stress fields there are dominated by the plane strain solution, as shown in Fig. 9(b). From these observations, the $J-Q$ annulus discussed in the previous sections may be valid there. On the free edge-surface, however, the stress fields (Figs. 10(c,d)) contain substantial plane stress components. The tangential stress difference between the finite element results and the plane strain reference solution is almost a linear function of the polar angle (Fig. 10(c)). This represents in fact the difference between the plane strain and the plane stress field. The difference increases with the applied loads. In the

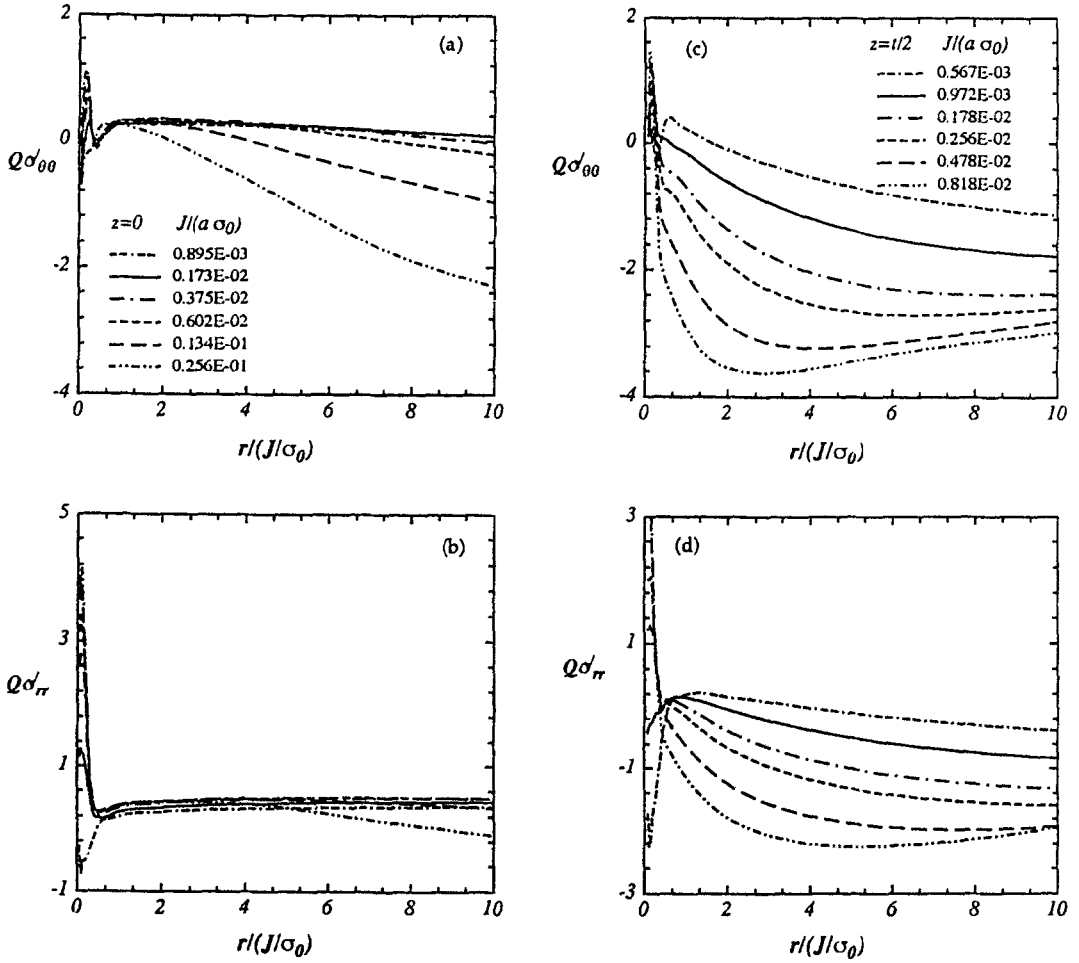

Fig. 12. Radial variations of the second-term of the hoop stress at the middle plane ($z = 0$) as well as near to the free surface ($z = t/2$) of the thick compact tension specimen (CT25) at $\theta = 3.2°$.

thin specimen, on the other hand, the stresses in the middle plane of the specimen can be described by the plane strain fields only if the applied loads are very low (Fig. 11(a)). The stress distributions in the whole specimen develop towards the plane stress fields quickly as the loads increase. The non-uniform distribution of the second terms in the three-dimensional crack fields can also be found in their radial variations (Fig. 12 for the thick specimen). Only at low load level are the radial distributions slightly dependent on the distance r. On the free edge-surface the second terms are a function of the distance and the loads. Recalling the difference between the plane strain and the plane stress solution, one may see that such distributions cannot be independent of the distance.

The variation of the stress triaxiality in the CT specimens implies that the thin specimen contains significantly lower constraint than the thick specimen. This point can also be observed in the Q-variations in the thickness direction plotted in Figs. 13(a,b). The curves vary with the load levels. The Q values are evaluated according to (3). For the stress fields containing substantial plane strain components, the absolute values of Q should be small. The figures show that the plane strain fields shrink with increasing load.

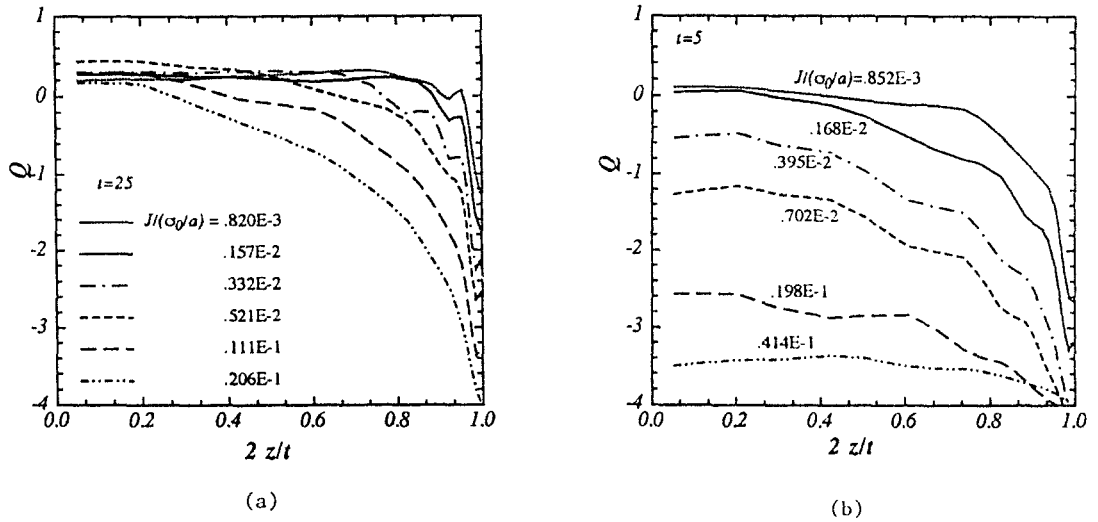

Fig. 13. Variations of the Q values in the specimen thickness at $r/(J/\sigma_0) = 2$ and $\theta = 3.2°$. (a) CT25; (b) CT05.

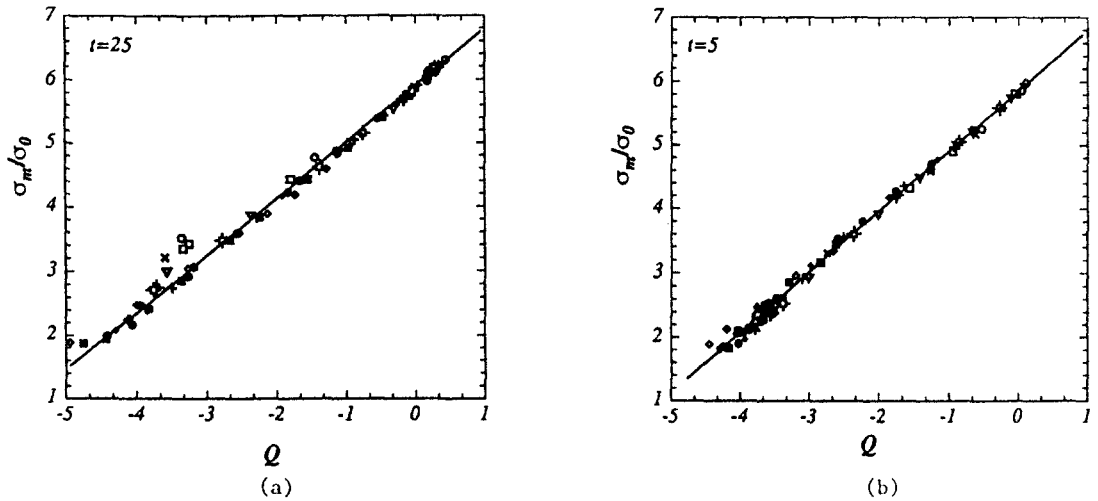

Fig. 14. The hydrostatic stress, σ_m/σ_0 at $r/(J/\sigma_0) = 2$ and $\theta = 3.2°$, as a function of Q. (a) CT25; (b) CT05.

The discussion above has shown that the three-dimensional crack tip fields generally have mixed plane strain and plane stress characteristics. Especially in the thin cracked panel, the fracture process is only characterised by the plane stress fields, as predicted in [21]. For this reason, it becomes interesting to know how the stress triaxiality at the crack tip can be characterised by the second parameter such as Q, which was introduced under pure plane strain conditions. Based on the discussions above, the characterisation of the hydrostatic stress should be a function of the specimen geometry as well as the material properties, that is

$$\sigma_m = \sigma_0 \Omega(Q, \text{ geometry, material properties}). \tag{12}$$

In this expression the stress triaxiality at $r = 2J/\sigma_0$ and $\theta = 0$ is explicitly independent of the applied loads. Equation (12) is plotted in Fig. 14(a) for the thick CT specimen and in

Fig. 14(b) for the thin one, respectively. It is interesting to observe that the stress triaxiality at the tip is essentially a linear function of Q. The Equation (12) can be re-written as

$$\frac{\sigma_m}{\sigma_0} = b_1 Q + b_0, \tag{13}$$

where the factors b_0 and b_1 are functions of the crack geometry and the material properties. Recalling the definition of the Q factor, one may see that b_0 is the triaxiality of the plane strain reference solution. In the present definition (3), it is the small-scale yielding results with $T = 0$. Our numerical calculations have shown that b_1 depends slightly on the geometry of the specimens. For the thick and thin CT specimens investigated in the present work, b_1 equals 0.945 and 0.988, respectively. For all conventional cracked geometries we have examined [19], b_1 is approximately equal to 1, i.e. $|b_1 - 1| \leqslant 0.1$. It is therefore confirmed that the Q value represents the local difference of the stress triaxiality at $r = 2J/\sigma_0$ and $\theta = 0$ in the three-dimensional crack fields. It gives a uniform relation between the stress triaxiality and Q. Equation (13) becomes trivial under plane strain small-scale yielding conditions.

5. Concluding remarks

In extensive numerical studies of Shih and co-workers [6, 7, 17, 18] the $J-Q$ annulus has been suggested for quantification of the crack-tip constraint effects. The many known results are restricted to the Ramberg–Osgood materials and to the crack-tip fields dominated by the plane strain solution. In the present work, we have presented detailed numerical results for a ductile engineering material. The three-dimensional crack tip fields containing substantial plane stress components under both small-scale and general yielding conditions have been investigated.

Due to high strain-hardening in the austenitic steel, the stresses reach a very high level at the crack tip. The Q values vary with the negative transverse T-stress in analogy to the Ramberg–Osgood materials. The positive T stress, however, acts on the crack stress fields under small-scale yielding almost as strongly as the negative T. Significant increments of the Q values are further observed under the general yielding conditions. Due to the low yield stress and high ductility, the Q values may reach several times those for a Ramberg–Osgood material [6, 17]. The stress triaxiality at the tip is a function of both specimen geometry and the load configuration. For the tensile panels (CCT and DECP), the Q variations show similar features and the Q values are slightly affected by the crack length, except the deep-cracked specimens with $a/W > 0.7$. The bending geometry shows a much higher constraint at the tip. A significant drop of the Q values can only be observed as $J/(\sigma_0 a) > 0.01$, except the shallow-cracked specimens with $a/W < 0.3$. It is important to point out that development of the fully plastic stress field is not uniform, so that a parameter evaluated behind the crack tip ($\theta = \pi$) may totally differ from that evaluated ahead of the tip ($\theta = 0$). It has been confirmed that the $J-Q$ description is equivalent with $J-T$ only if the influences of the specimen geometry to the crack-tip stress distributions are negligible. In general yielding cases, T loses its connection to the crack-tip fields and the prediction from $J-T$ may significantly deviate from the full stress fields.

In the three-dimensional crack tip front fields, we have shown that the crack-tip front fields generally contain substantial plane stress components, the second terms of the stresses vary significantly along the crack-tip front and with the distance from the crack tip. It seems difficult for one additional parameter to control the second-order stress fields under general

yielding conditions. Q represents only the stress state at the evaluation point. In conventional cracked geometries the stress triaxiality at $r = 2J/\sigma_0$ and $\theta = 0$ can be approximated by a linear function of Q. In the cracked geometries investigated, Q is essentially equal to the difference of the local hydrostatic stress from the reference stress fields.

References

1. A.M. Al-Ani and J.W. Hancock, *Journal of the Mechanics and Physics of Solids* 39 (1991) 23–43.
2. C. Betegón and J.W. Hancock, *Transaction of ASME, Journal of Applied Mechanics* 58 (1991) 104–110.
3. D.M. Parks and Y.-Y. Wang, in *Analytical, Numerical and Experimental Aspects of Three Dimensional Fracture Processes*, ASME, AMD-91, A.J. Rosakis et al. (eds.), (1988) 19–32.
4. Y.-Y. Wang, in *Constraint Effects in Fracture, ASTM STP 1171*, Philadelphia (1993) 120–138.
5. D.M. Parks, in *Topics of Fracture and Fatigue*, A.S. Argon (ed.), Springer-Verlag, New York (1992) 59–98.
6. N.P. O'Dowd and C.F. Shih, *Journal of the Mechanics and Physics of Solids* 39 (1991) 989–1015.
7. Ibid., 40 (1992) 939–963.
8. N.P. O'Dowd and C.F. Shih, *Fracture Mechanics: Twenty-Fourth Volume, ASTM STP1207* (1994) 21–47.
9. J.R. Rice, *Transactions of ASME, Journal of Applied Mechanics* 35 (1968) 379–386.
10. W. Brocks and W. Schmitt, 'The second parameter in J-R curves: Constraint or triaxiality?' Presented at Second Symposium on Constraint Effects in Fracture, Nov. 17–18, 1993. To appear in ASTM STP.
11. M.L. Williams, *Transaction of the ASME: Journal of Applied Mechanics* 24 (1957) 111–114.
12. L. Xia, T.C. Wang, and C.F. Shih, *Journal of the Mechanics and Physics of Solids* 41 (1993) 665–687.
13. A. Cornec and K.-H. Schwalbe, 'Charakterisierung eines austenitischen Stahles (X6CrNi1811) mit den Methoden der Fliessbruchmechanik unter besonderer Betonung des CTOD-Konzeptes', Final Report for the DFG-Project with the Contract-No. Schw190/14, Institute for Materials Research, GKSS Research Center, Geesthacht, Germany (1990).
14. *ABAQUS User Manual*, Version 5.2, Hibbitt, Karlsson & Sorensen, Inc., Providence, R. I. (1992).
15. R.M. McMeeking and D.M. Parks, *Elastic-Plastic Fracture Mechanics, ASTM STP 668* (1979) 175–194.
16. H. Yuan and G. Lin, *International Journal of Fracture* 61 (1993) 295–330.
17. C.F. Shih and N.P. O'Dowd, 'A fracture mechanics approach based on a toughness locus', presented at International Conference Shallow Crack Fracture Mechanics, Toughness Tests and Applications, Cambridge, UK, 1992.
18. C.F. Shih, N.P. O'Dowd, and M.T. Kirk, in *Constraint Effects in Fracture, ASTM STP 1171* (1993) 2–20.
19. H. Yuan, 'Effects of biaxial loading on three-dimensional crack front fields' presented at 10th European Conference on Fracture, Berlin, 1994.
20. P.S. Leevers and J.C. Radon, *International Journal of Fracture* 19 (1983) 311–325.
21. T. Nakamura and D.M. Parks, *Journal of the Mechanics and Physics of Solids* 38 (1990) 787–812.
22. T.L. Sham, *International Journal of Fracture* 48 (1991) 81–102.